This is a preprint version of the paper published in Journal of Analytical and Applied Pyrolysis 143 (2019) 104685

Triethanolamine (TEA) effect on the pyrolysis of metal propionate-based solutions shown by thermal analysis

Silvia Rasi[1,2], Susagna Ricart[2], Xavier Obradors[2], Teresa Puig[2], Pere Roura-Grabulosa[1] and Jordi Farjas[1]

[1] University of Girona, Campus Montilivi, Edif. PII, E17003 Girona, Catalonia, Spain
[2] Institut de Ciència de Materials de Barcelona, ICMAB – CSIC, Campus UA Barcelona, E-08193 Bellaterra, Catalonia, Spain

*Corresponding author: Silvia Rasi (silvia.rasi@udg.edu ; srasi@icmab.es)

Abstract

The effect of triethanolamine (TEA) on single-salt propionate-based solutions used to prepare $YBa_2Cu_3O_{7-\partial}$ (YBCO) has been studied through thermal analysis, for film and powder samples. Decomposition has been followed by thermogravimetry (TG) coupled to differential scanning calorimetry (DSC) and evolved gas analysis (EGA-MS and TG-FTIR), while chemical characterization has been carried out by FTIR, XRD and EA. The addition of TEA has little effect on the decomposition of Ba-Prop-Ac. Conversely, the thermal behavior of $CuProp_2$ and $YProp_3$ film with TEA becomes more gradual and less affected by a change of atmosphere than the TEA-free case. This is explained by the fact that the decomposition mechanism is driven by the formation of an ester between the propionate groups and the TEA's OH groups, which is promoted by inert atmospheres and temperatures above 200°C. Just as the single salt precursors, the Ba and Y films show residual organic material at 500°C in thick films decomposed in O_2.

Keywords: Triethanolamine complexes; thermogravimetric analysis; metal propionates, EGA-MS; TG-FTIR

1. Introduction

Chemical solution deposition (CSD) methods [1] of metalorganic compounds have attracted attention due to their easy accessibility and low costs when compared to physical methods in order to fabricate coated conductors (CCs) [2]. CSD methods are based on the formulation of a solution that can be deposited on a surface to undergo two main thermal steps: pyrolysis, during which all the organic material is removed and intermediates inorganic phases are formed; and growth, at higher temperatures, during which the oxide layer crystallizes from these intermediates.

In the case of advanced oxides that involve more than one metal precursor, such as the case of superconductive tapes, one of the main challenges of CSD methods is to achieve homogeneous distributions of all starting species by avoiding phase segregation, buckling and cracks [3] during the thermal treatments, since they can act as pores for magnetic granularity [4,5], leading to a drop of the critical current of the superconductor. Therefore, good control of the final

properties of the film relies on a good control of the deposition and pyrolysis stages, where these defects arise from the shrinkage of the film following decomposition. In fact, thermal treatments are normally long in time to favor a slow gas release so to reduce tension, and get stress-free films; but time constitutes a problem for industrial applications. Therefore, to ensure stability in the deposited layer, additives [6] such as triethanolamine (TEA) are added, since they help reducing stress and improve rheological properties, by increasing the viscosity of the initial solution.

In particular, besides being used for preparation of cosmetics and surfactants, cement and nanostructures, TEA is of special interest because of its chelating properties [7,8]; in fact, as an aminoalcohol, its properties lie between those of amines and alcohols, acting as both N-donor and O-donor thanks to the three OH groups. Therefore, while increasing viscosity, TEA is expected to form complexes and to increase the stability of the metal carboxylate salts in solution. In fact, it is known that copper can form stable complexes with nitrogen and oxygen donors [9–11]; similarly, Y^{3+} has been reported to form complexes with TEA [8] while Ba^{2+} is not expected to coordinate with TEA [12,13].

Regarding TEA thermal decomposition during pyrolysis [14,15], the aspect ratio is expected to play a role [16]: in fact, when in the form of films, TEA is likely to evaporate before reaching its decomposition temperature (250-300°C) thanks to the high surface to volume ratio. When it is placed inside a crucible, evaporation is significantly slowed down so it can be heated to higher temperature (above 300°C) where it decomposes releasing acetaldehyde (CH_3CHO), CO_2, ammonia (NH_3) and ethylene oxide (CH_2OCH_2) [14,16]. On the other hand, metalorganic complexes of TEA are expected to decompose following several decomposition steps [17] that start with the loss of small TEA units and end with the metal salt decomposition.

Finally, metal propionate salts have been shown to decompose following a radical path in inert atmosphere and high temperatures, releasing a symmetrical ketone (3-pentanone) and CO_2 [18–23] and forming the corresponding oxides (for $YProp_3$) or carbonates (for $BaProp_2$) by 500°C. In O_2, oxidative degradation of the ligand is expected to occur at low temperature releasing propionic acid, acetaldehyde, CO_2 and water, but without changing the final phases [24–26]. Conversely, for $CuProp_2$, propionic acid is expected to be the main volatile independently of the atmosphere [25], followed by acetaldehyde and CO_2 to give the corresponding oxide in film, and metallic copper as powder.

In this work, we will apply thermal analysis (TA) on film samples, despite the limitation of the small sample amount in films which pushes TA techniques to their limits. We will provide a closer look on the pyrolysis of FF-$YBa_2Cu_3O_{7-\partial}$ (YBCO) films [27–29], a high temperature superconductor (HTS)[30,31], by studying in-situ the effect of TEA on each of the three metalorganic salts used for the fabrication of YBCO with chemical methods: $YProp_3$ [22,24,32,33], $CuProp_2$ [20,34–36], Ba-Prop-Ac [18]. Humid O_2 atmospheres will be studied in comparison to inert atmospheres, as the former are normally used during YBCO pyrolysis. Evolved gas analysis (EGA-FTIR and EGA-MS) coupled to TG-DSC will be used to reveal the gas species evolved during decomposition. XRD, FTIR and EA will be used to ex-situ characterize the solid residue at different stages of the thermal degradation. We will show that TEA changes the decomposition mechanism of the carboxylate salt and that it can affect the final products in terms of C amount. Finally, we will use TA to discuss decomposition in the context of the nature of TEA interaction with the metalorganic salt.

2. Materials and methods

2.1 Sample preparation

Three separate solutions were prepared starting from metal acetate precursors: YAc_3 (Sigma Aldrich, 0.25M), $BaAc_2$ (Sigma Aldrich, 0.5M) and $CuAc_2$ (Sigma Aldrich, 0.75M), were separately dissolved in a 1/1 mixture of propionic acid (Merck, ≥99%) and MeOH (VWR, ≥99.8%), to reach a stoichiometric ratio of 1/2/3 of, respectively, Y/Ba/Cu (sol. **A**, **B** and **C**). A 5% v/v of triethanolamine (TEA, Merck, >99%) was added to each solution so that the final molar proportions Y/Ba/Cu/TEA were close to 1/2/3/1.5. For comparison, solutions without propionic acid were prepared from the corresponding $MProp_x$ salts obtained drying the previous solutions (**A** and **C**); these $MProp_x$ salts were dissolved in MeOH with 5% TEA, keeping the same stoichiometric ratio: **A'** ($YProp_3$/TEA in MeOH) and **C'** ($CuProp_2$/TEA in MeOH). Film samples were prepared from these solutions by drop casting over 10x10 mm $LaAlO_3$ (LAO) substrates; they were dried at 80°C for a few minutes to remove most of the solvent while avoiding TEA evaporation and then decomposed in humid O_2 for thermal analysis experiments. The film thickness (H) was estimated with the following equation: $H = {}^{m}/_{d \cdot A}$, where *m* is the fil mass after decomposition, *d* is the particle density of Y_2O_3, CuO or $BaCO_3$, and *A* is the surface area of the substrate. The corresponding powders were obtained by peeling off the deposited dry films and they were placed in a 70-µl alumina pan to study their decomposition in inert atmosphere.

2.2 Characterization methods

Thermogravimetric (TG) analyses were performed in a Mettler-Toledo thermobalance, model TGA/DSC1, at 5°C/min. Experiments performed in humid O_2 atmosphere were carried out with a 55-ml/min flow of reactive gas (humid O_2) and 15 ml/min of protective gas (air). Experiments run in N_2 atmosphere were performed with flows of 70 ml/min of the dry inert gas.

TG-FTIR experiments were carried out connecting the gas outlet of the TG equipment to the gas inlet of an infrared (IR) spectrometer with a 30-cm steel tube kept at 200°C. The IR analyzer is a Bruker Alpha II spectrometer equipped with a gas cell. Both gas cell and tube are kept at 200°C to prevent volatile condensation.

EGA-MS experiments were run placing the film on an alumina holder inside a quartz tube closed on one end. This quartz tube extremity is surrounded by a low-resistance furnace. A K thermocouple is in tight contact with the film substrate and used to control the temperature program. The open end of the quartz tube is connected to the vacuum system and to a quadrupole mass spectrometer (MS-Q) analyzer by MKS instruments, model Microvision Plus. The vacuum was reached by pumping the system to P_{tot}~10^{-7} bar with the aid of a turbomolecular pump in series with a rotative pump.

Elemental analysis (EA) was performed with a Perkin Elmer EA2400 series elemental analyzer. Detection limits are in the range of 0.72% for C and 0.2% for H values. X-ray measurements were carried out with a Cu-Kα X-ray beam of a D8 ADVANCE diffractometer from Bruker AXS, with a voltage of 40 kV and a 40-mA current. Infrared spectra of solid samples were collected with an ALPHA spectrometer from Bruker, in attenuated total reflection (ATR, model Platinum).

3. Results

*3.1 Thermal decomposition of Ba-Prop-Ac /TEA (sol. **B**)*

Ba-Prop-Ac/TEA solution (sol **B**) exhibits the simplest behavior of the three under study, and for this reason is discussed first. The FTIR spectra in Fig. 1a of the dry films show characteristic TEA vibration bands, and the partial replacement of acetate groups by propionates [37] with formation of a mixed Ba-Prop-Ac complex [18,26]. The XRD of the dry film (Fig. 1b) is in agreement with that of the mixed carboxylate salt Ba-Prop-Ac found in [26], suggesting that no new TEA-Ba complex is formed.

The thermogravimetric curve shown in Fig.2 exhibits three main mass loss steps: a first one between 50 and 150°C, which corresponds to water and propionic acid evaporation. A second TG step with 27.7% mass loss (theoretical for TEA removal: 28.4 and 29.28% starting from $BaProp_2$ and $BaProp_8Ac_6$, respectively) takes place between 150-300°C. In the low-temperature region of this range (150-210) a gradual mass loss takes place while the FTIR of the solid residue shown in Fig. 1 (210°C) reveals that while TEA is evolving, an IR band at 1735 cm^{-1} emerges. This band can be assigned to an ester bond between propionic acid and TEA's OH groups. Indeed, this band also appears in a solution of only TEA and propionic acid (see Supp. Info, Fig. S1).

Since during decomposition of the barium carboxylate salt, propionic acid can evolve up to 150-200°C [26], it is reasonable to believe that the propionate units involved in the esterification come from the solvent. In fact, if they came from the salt, the last mass loss in Fig. 2 relative to the decomposition of Ba-Prop-Ac would be smaller. An endothermic DSC signal centered at 220°C (Fig. 2) is also consistent with some TEA evaporation, in agreement with the temperature range observed for TEA evaporation in films by [16]. However, it was not possible to identify the TEA by infrared in the gas phase due to the little amount evaporating which is further reduced by its condensation along the path, a phenomenon already noted by [16]. Additionally, between 210 and 300°C, the high temperatures promote TEA decomposition and in fact the infrared of the gaseous products shows TEA's decomposition products: ammonia and acetaldehyde (TG-FTIR in inset of Fig. 2).

Simultaneously, the XRD curve in Fig. 1b at 220°C shows new peaks toward lower angles, indicating a change in the barium carboxylate structure after solvent and water elimination taking place during TEA removal. As expected, also its carboxylic stretching bands have shifted from 1512 cm^{-1} to 1549 cm^{-1} during the 200°C-interval before oxidative degradation begins, due to dehydration and recrystallization [26]. The main TEA absorptions and the ester peak disappear after this stage, leaving a FTIR spectrum at the beginning of the third stage (280°C) that is identical to that of the barium carboxylate salt [26].

The third TG step, in Fig. 2, occurs between 300-500°C and corresponds to the decomposition of Ba-Prop-Ac to $BaCO_3$, with a characteristic DSC exothermic peak [26] and with a ratio $m_{500°C}/m_{300°C}$ for this step of 71.2% (theoretical: 69.9 and 72.7% starting from $BaProp_2$ and $Ba_7Prop_8Ac_6$, respectively). Acetaldehyde, CO_2, methane and CO are detected in humid O_2, in agreement with [26].

The expected final mass with respect to the initial dry film considering a simple addition of all components in solution ($BaProp_2$/Ba-Prop-Ac + TEA) is between 49.85 and 51.41%, in agreement with the thermogravimetric curve that lies at 51%. EA results in Table 1 at 500°C shows a C% value slightly above the expected one for $BaCO_3$, which might be in agreement with the gray color of the final product (expected to be white) due to residual carbon remaining, just as in the case of Ba-Prop-Ac alone. With respect to Ba-Prop-Ac alone (see Supp. Info, Fig. S4), the thermogravimetric behavior is very similar as well as the final decomposition temperature. Also,

the EGA-MS analysis of a film of solution **B** decomposed in vacuum (See Supp. Info, Fig. S7) yields identical results to the EGA-MS of Ba-Prop-Ac without TEA [26], confirming that TEA evaporation in vacuum takes place before the salt decomposition.

*3.2 Thermal decomposition of $CuProp_2$ /TEA (sol. **C**)*

Decomposition in oxidative atmosphere

The FTIR analysis of the dry film from solution **C**, Fig. 3a, shows the appearance of the TEA IR bands and of $CuProp_2$ vibrations [20,25,38], in agreement with the expected replacement of acetate groups by propionates of the solvent when this is in excess [37] (details in Fig. S2). But the XRD pattern is significantly different from that of $CuProp_2$ [25] (see Fig. S2), suggesting a possible coordination of TEA with $CuProp_2$.

The TG analysis in humid O_2 reported in Fig. 4 shows that after solvent removal and dehydration below 150°C, four overlapping steps centered at 155, 210, 245 and 328°C take place: they correspond to exothermic peaks (DSC signal in Fig. 4, top). The gas species evolved during decomposition in humid O_2 consist of propionic acid, acetaldehyde, CO_2 and NH_3 (Fig. 4). Since only NH_3 can be easily assigned to TEA decomposition, while all other gas species are the expected volatiles for both TEA and for $CuProp_2$ decomposition, interpretation of TG-FTIR results is not straightforward.

The four mass steps can be grouped into two main stages which correspond to $CuProp_2$ accompanied by some TEA release, and TEA decomposition, respectively.

In particular, the first stage, between 100-230°C, matches with $CuProp_2$ decomposition and TEA removal: the FTIR (Fig.3a) of the solid residues quenched at 185°C shows that the main TEA vibrational band at 1082 cm^{-1} is decreasing; simultaneously the $CuProp_2$ reflections are detected by XRD (Fig.3b) [25,39] decreasing while it decomposes to propionic acid and CO_2 (TG-FTIR analysis in Fig. 4) according to the expected hydrolysis and degradative oxidation path [25]. Between 95 and 185°C, an IR band at 1735 cm^{-1} appears in the solid residue, Fig. 4.4a, which may be assigned to some TEA/propionate ester bond, although a similar absorption band was observed for the $CuProp_2$ decomposition in correspondence of its reduction to Cu(I).

The second stage, between 230-500°C, is affected by the fact that TEA evaporation evolves into decomposition at these temperatures in oxygen: between 230°C-270°C, CO_2, acetaldehyde and NH_3 from oxidative degradation are detected while Cu(II) is reduced to Cu_2O and Cu (XRD in Fig. 3). The presence of CO_2 between 210-250°C (Fig. 4) could be an indication of this redox reaction due to carbon left by TEA. The last mass loss, releasing CO_2 at 328°C, is again indirectly attributable to the presence of TEA, since the end of decomposition is shifted to almost 100°C higher with respect to the case of $CuProp_2$ film alone, for which it is over by 250°C (See Fig. S4 in supp. info). In fact, at higher temperatures in O_2, a TG-FTIR experiment run on TEA alone (Fig. S8) shows that TEA is oxidized to CO_2. The temperature range of this second TG stage is also in agreement with the decomposition temperatures found for other Cu-TEA complexes [9,17,40,41]. The final product consists of CuO, as shown by XRD and FTIR in Fig. 3, and no carbon or hydrogen is detected by EA (Table 1). The experimental final mass lies at 32%, slightly above the expected value of 28.9 %. A solution of $CuProp_2$ with 5% TEA in only MeOH (sol. **C'**) yields the same TG-FTIR behavior and for comparison it is shown in Fig. 4.

Decomposition in inert atmosphere

It is known that both $CuProp_2$ [25] and TEA, independently, exhibit a strong tendency to evaporate at low total pressure. But when decomposition of solution **C** is carried out in vacuum (Fig. 5, bottom, EGA-MS experiment), $CuProp_2$ evaporation is considerably reduced. In fact, unlike the case of $CuProp_2$ alone in the form of film, with the addition of TEA, no $CuProp_2$ is recovered from condensation along the quartz tube, and the mass loss is not significantly higher than the expected value; the final product at 500°C consists of a shiny metallic copper film, indicating that $CuProp_2$ evaporation is definitely reduced in vacuum when TEA is added.

However, from the EGA-MS analysis in Fig. 5, only a low-temperature stage is observed: the most intense peak, at 200°C, still shows evolution of propionic acid (m/z=45, 29, 28, 27) corresponding to $CuProp_2$ decomposition, but an excess of m/z=28 (CO, N_2 or C_2H_4) with respect to the case without TEA is detected. This might be an indication that a TEA effect is present up to 200°C, and thus that also its evaporation is reduced when $CuProp_2$ is added, due to the coordination between TEA and Cu^{2+} of the carboxylic salt. To better understand the thermal decomposition of sol. **C** in inert atmosphere, the effect of evaporation should be avoided by *i)* studying decomposition in powders instead of films and *ii)* under an atmospheric pressure of an inert gas, such as N_2, instead of at low total pressures.

The TG behavior during decomposition in N_2 of the corresponding powder obtained from solution **C** is reported in Fig. 5. Endothermic events can be observed in the first stage, before 230°C, in correspondence of propionic acid and CO_2 release, coming from the beginning of $CuProp_2$ decomposition in N_2. The main difference from the humid-O_2 case lies in the formation of a TEA-propionate ester evolving at 260°C, in the second stage; this ester is ethyl propionate, detected among the volatiles by TG-FTIR (inset in Fig. 5) along with some TEA, while CH_3CHO and NH_3 that would come from TEA decomposition alone are no longer noticeable.

This ester (ethyl propionate) comes from a decomposition process; thus, it is different from the ester observed by FTIR (band at 1735 cm^{-1}) in the solid residue at low temperatures in sol. **B**, Fig. 1a (but also later on in sol. **A**, section 3.3) which instead comes from esterification between TEA and propionic acid (see also Fig. S1). This difference will be further commented in section 3.3, in the case of sol. **A**. Indeed, ethyl propionate can be ascribed to the decomposition path described by the following reaction scheme:

$$^{x}/_{3}N(C_2H_4OH)_3 + M(C_2H_5CO_2)_x \rightarrow xC_2H_5C(=O)–OC_2H_5 + MO_x + {}^{x}/_{6}N_2 \qquad (i)$$

Where M is the metal cation (Cu or Y).

Note that, in vacuum, formation of ethyl propionate is probably disfavored by the low decomposition temperature (200°C) and the tendency for both TEA and $CuProp_2$ to evaporate at low total pressures. Note also that in N_2, $CuProp_2$ in powder form and without TEA, decomposes with a sharp mass loss followed by copper reduction to Cu(0) (see Fig. S4); conversely, in sol. **C**, the presence of overlapped decomposition between TEA and the carboxylic salt makes decomposition smoother.

Finally, note that, according to reaction scheme *(i)*, generation of ethyl propionate as volatile corresponds to the formation of the oxide CuO instead of Cu. Indeed, in the same decomposition conditions (powders in N_2) only Cu and Cu_2O are observed during decomposition of $CuProp_2$ without TEA [25] at 360°C; conversely, during decomposition of $CuProp_2$ with TEA also CuO is detected at 360°C (sol. **C**, see Fig. S3 in supp. Info), which indicates that less reduction occurs at intermediate temperatures. But the quenched $CuProp_2$/TEA powder at 360°C (Fig. S3) is black even though the main XRD reflections belong to Cu(0), maybe due to residual carbon. It is reasonable to believe that when TEA decomposes simultaneously to $CuProp_2$ forming the ester

(stage II of Fig. 5) instead of propionic acid, it prevents Cu(II) reduction in N_2 through reaction scheme *(i)*.

Once formed, this copper oxide is eventually reduced to Cu(0) in inert atmosphere, further helped by the residual carbon, which evolves as CO_2. CO_2 is indeed detected between 480-500°C (see inset in Fig. 5). The final mass lies at 29.6%, higher than the expected value for Cu, indicating presence of residual carbon, just as found for the case of the thermal decomposition of powders of $CuProp_2$ in N_2 [25].

Thus, formation of ethyl propionate requires higher temperatures than the low-temperature range (100-200°C) where $CuProp_2$ is expected to decompose in O_2 (see Supp. Info, Fig. S4, and for this reason, its contribution to decomposition in humid O_2 is minor (and propionic acid remains the main volatiles). Due to the fact that an increase in $CuProp_2$ film thickness causes a shift of decomposition to higher temperatures [25], some ethyl propionate is also detected even in humid O_2 above 200°C for CuO films thicker than 3 µm. Finally, even increasing the TEA/Cu ratio in solution to 1/1 in order to push the equilibrium towards the ester instead of towards propionic acid is unsuccessful: the main volatile in humid O_2 is still propionic acid (not shown).

*3.3 Thermal decomposition of $YProp_3$ /TEA (**A**)*

Decomposition in oxidative atmosphere

As shown from the TG curve of Fig. 6, solution **A** is hard to dry at low temperature, since evaporation and decomposition overlap: after drying at 80°C, the film is still a colorless viscous liquid and the FTIR spectrum of Fig. 7a shows the TEA IR bands and those of $YProp_3$ [24] (and Fig. S2). To remove the contribution of the solvent and for the sake of clarity, the time-resolved evolution of the volatiles reported in the TG-FTIR analysis of Fig. 6 (dotted lines) is relative to solution **A'**. In fact, **A'** is prepared by dissolving $YProp_3$ in MeOH, instead **A** by dissolving YAc_3 in a mixture of propionic acid and MeOH. For both **A** and **A'**, the expected final mass for the mixture of $YProp_3$ and TEA to yield Y_2O_3 is 21.2%, which is in agreement with the experimental value of 24.5% of Fig. 6, considering that the FTIR analysis (Fig. 7a) of the solid residue at 600°C reveals the presence of residual $Y_2O_2CO_3$.

Three main stages can be identified when decomposition is carried out in humid O_2.

The first one, between 50 and 150°C (Fig. 6), involves dehydration and evaporation of the solvent (propionic acid). In fact, in the solid residue, Fig. 7a, the main propionic acid and H_2O IR absorptions decrease going from 90°C to 150°C. In particular, the disappearance of the broad band between 2500-400 cm^{-1} is a sign of solvent removal, but also the general intensity decrease in the 1300-1700 cm^{-1} region (where the $YProp_3$ bands are) is due to the solvent. This step also corresponds to the appearance of an ester band at 1736 cm^{-1} in the FTIR of the solid residue, as noticed also for sol. **B**. This band probably arises because the temperature increase promotes esterification between TEA and propionic acid. In **B** this was explained by the fact that no coordination took place between TEA and Ba ions, thus all TEA (Ba/TEA=2/1.5) is free to react with the solvent (prop. acid). In sol. **A**, there is always some free TEA since TEA is in excess with respect to Y^{3+} (Y/TEA=1/1.5). Conversely, esterification of the solvent in **C** is minor, due to the fact that Cu is in excess with respect to TEA, and TEA is coordinated to $CuProp_2$.

The second stage, between 150-300°C, corresponds to 37% mass loss. The main volatiles detected are propionic acid and ethyl propionate, but also TEA's vibrational bands [16] are observed. The propionic acid comes from $YProp_3$ decomposition in humid O_2; ethyl propionate,

already observed also for solution **C**, originates from the simultaneous decomposition of both TEA and $YProp_3$ according to reaction scheme (*i*): in fact, the yttrium propionate IR bands of the solid residue, Fig. 7a, start to decrease already at 150°C and by 240°C their intensity has significantly decreased. In addition, the FTIR of the solid residue, Fig. 7a, reveals that TEA contribution disappears somewhere between 240 and 340°C. Lastly, the fact that TEA's vibrational bands are also observed among the volatiles is in agreement with the fact that evaporation takes place in films before 200°C and that there is an excess of TEA with respect to Y (1.5/1, respectively).

The last stage of Fig. 4.9, between 300-600°C, mostly includes $YProp_3$ decomposing to Y_2O_3, since most TEA has been previously consumed.

In fact, first, between 300 and 400°C, the remaining $YProp_3$ decomposes to Y-oxycarbonate, $Y_2O_2CO_3$, observed by FTIR in Fig. 7a and in agreement with [24,32,33,42]. This occurs upon release of CO_2, acetaldehyde and 3-pentanone (TG-FTIR in Fig. 6, top). Note that the CO_2 peaks between 300-330°C could also be ascribed to the end of TEA decomposition, since at higher temperature its oxidative degradation takes place [16] releasing CO_2 (Fig. S8). However, the X-ray analysis reported in Fig. 7b shows the presence of amorphous species in this last stage (300-600°C), between $YProp_3$ decomposition and until Y_2O_3 crystallization takes place. Finally, between 400-500°C, $Y_2O_2CO_3$ decomposes to Y_2O_3 (identified by XRD, Fig. 7b) with CO_2 release. The EA results in Table 1 confirm the presence of carbon in the final product, due to the small remaining amount of $Y_2O_2CO_3$ with respect to Y_2O_3, similarly to the case of $YProp_3$ without TEA [24].

Note that, the ester band in the solid residue (~1736 cm^{-1}, Fig. 7a) disappears before 230°C, while ethyl propionate is detected among the volatiles between 200-350°C. As already previously mentioned, these two esters are attributed to different processes. Ethyl propionate is ascribed to reaction scheme *(i)*. In fact, the boiling point of ethyl propionate is just below 100°C, thus as soon as it is formed it is expected to evaporate; therefore, ethyl propionate cannot correspond to the ester IR band of the solid residue at 1736 cm^{-1}. This band might arise majorly from esterification of propionic acid (solvent) in the low-temperature region before its evaporation is completed.

Decomposition in inert atmosphere

In inert atmosphere of N_2 (Fig. 8), decomposition of the powder sample from sol. **A** follows the same general behavior: TEA still evolves in the low-temperature stage at 250°C while CO_2 is detected at higher temperatures, namely 310, 340, 430°C, along with ethyl propionate.

But the EGA-FTIR analysis of Fig. 8 (top, inset) shows that the ethyl propionate contribution increases in N_2: in fact, this ester becomes the main volatile, while the contribution of TEA and 3-pentanone decreases with respect to the film decomposition in humid O_2 (the only propionic acid detected seems to come from solvent evaporation below 200°C) and no ammonia can be detected. This is probably related to several facts, such as that 1) the lack of oxygen delays the precursor decomposition, resulting in a major overlap of TEA and $YProp_3$ decomposition, which in turns favors esterification; 2) that the bulk form prevents TEA volatilization, which results again in a major overlap of TEA and $YProp_3$ decomposition. In fact, the behavior of the two TG curves of sol. **A** (hum. O_2 and N_2) compared in Fig. S4, is quite similar, but the first mass loss (TEA) is shifted to lower temperatures in films in humid O_2 since in films volatilization in enhanced with respect to decomposition. 3) reaction scheme (i) occurs through a radical reaction, which is favored by inert furnace atmospheres.

Therefore, reaction scheme *(i)* summarizes the driving reaction for decomposition of $TEA/MProp_x$ species in N_2.

The EGA-MS analysis in Fig. 8, bottom, performed on a film of sol. **A** decomposed in vacuum supports the TG-FTIR results, showing the presence of at least 2 stages of decomposition

between 250-400°C, while for the $YProp_3$ alone only one (at 360°C) is present [24]. The two peaks, centered at 280 and 360°C, include fragments that can be related to both ethyl propionate (m/z=29, 57) and 3-pentanone (m/z=57,29); but they both show the evolution of CO_2 (m/z=44), a signature of the occurrence of the 3-pentanone decomposition path typical of $YProp_3$ in vacuum [21,24]. Then, at 400°C, m/z=28 is detected, which could be assigned to C_2H_4, N_2 or CO. This excess of m/z=28 is not detected during the decomposition of $YProp_3$ without TEA, in vacuum; thus, it is an indication that less TEA evaporation occurs at these low total pressures as a consequence of its coordination with the metal carboxylate salt. The FTIR of the final product shows residual -C=O bands (supposedly from $Y_2O_2CO_3$), and it is very similar to that of the isolated $YProp_3$ decomposed in vacuum [24].

4. Discussion

Thermal analyses are a useful tool to study the effect of adding TEA to the three different metalorganic solutions: i) the well-defined TG mass losses, ii) the fact that the mass loss is the sum of all TEA and the metal salt in solution, iii) detection of TEA or its decomposition products among the volatiles, iv) the endothermic signal of the TEA evaporation step and v) the same TG, EGA-MS behavior and final decomposition temperature with respect to the $MProp_x$ without TEA, suggest that in the case of $BaProp_2$ there is no coordination with TEA, as predicted by [12].

Conversely, TEA changes Cu and Y decomposition pathways, partly because of TEA coordination with Y and Cu, but not with Ba; and partly because of the overlap of the two processes, namely the decomposition of the metalorganic salt and that of TEA (Ba salt decomposes at higher temperatures) which results in less separable mass losses.

But the decomposition mechanism follows from the tendency to either break the Cu—OC=O bond to form the corresponding acid, or the YO—C=O bond for the esterification reaction. In fact, for the copper case, the low-temperature mechanism with propionic acid formation is still faster and preferred in humid O_2, thus $CuProp_2$ decomposition is almost over when TEA's start. But in N_2, $CuProp_2$ can survive to higher temperatures (260°C) for the ester to be produced. For the $YProp_3$ case, since its decomposition temperature is higher than that of $CuProp_2$ in humid O_2, esterification is more significant. This ester is not observed in TEA decomposition alone [16], nor it is formed in the TEA-free solutions of the three metalorganic salts [24,25]; it follows that the atmosphere has a different effect on decomposition when TEA is added to the carboxylate salt. The barium salt oxidative degradation is based on the preferred cleavage of the MOC(=O)—C bond, as it tends to form BaC_2O_4 and $BaCO_3$ which only later on (T>>600°C) decompose to BaO [18,43]: that and the fact that its decomposition temperature and TEA's are so far apart, results in very little ester being formed.

It follows that the atmosphere has a different effect on decomposition when TEA is added to the carboxylate salt, since it changes the decomposition temperature range of the carboxylate salt, while it has no effect on the evaporation of TEA; i.e., it controls the overlap of the two processes (decomposition of TEA and of the salt) which eventually affects the degree of esterification and decomposition pathway. Similarly, the sample geometry, film versus powder, can promote or impede, respectively, TEA evaporation, and thus control the overlap of the two processes.

However, the change in decomposition temperature due to a change of atmosphere is more significant for the pyrolysis of the single-salt solutions without TEA than in the case of single-

salt solutions with TEA; this is probably a consequence of the fact that the esterification path can partly take place also in humid O_2, although in dry N_2 it is the predominant decomposition path.

In the framework of CSD methods, some effects need to be acknowledged when TEA is added: a shift in the final decomposition temperature with respect to the metalorganic salt without TEA, of 100°C and 50°C for the Cu and Y case, respectively; a slightly higher amount of residual carbon might remain at 600°C for the Y case, in humid O_2. Similarly, the presence of TEA causes an unexpected redox-reaction pattern not observed for the $CuProp_2$ alone [25]. In fact, reduction of Cu(II) occurs during decomposition in humid O_2 for sol. **C** ($CuProp_2$/TEA), due to the residual carbon from TEA; but this copper is eventually oxidized to CuO, which is the final product at 500°C. Conversely, in N_2, more Cu(II) reduction is expected during decomposition, but instead reaction scheme *(i)* generates CuO during pyrolysis; eventually this CuO undergoes reduction to Cu, which is the final product at 500°C.

Although only a fixed TEA amount was studied in this work, the M/TEA molar ratio can also play a role, influencing the amount of overlapped decomposition. In a combined solution of all the three analyzed, we would expect the TEA to mostly influence the copper and yttrium carboxylate decomposition. Perhaps the key aspect emerging from the thermogravimetric analysis is that, when TEA and the metal carboxylate display similar decomposition temperatures, the additive can provide smoother mass losses which translate into a gradual gas release. That is also reflected in the smaller effect of a change of atmosphere on the TG curves, unlike the case of the isolated salts. Similarly, the effect of switching from films to powders is less pronounced than for the isolated salts (especially for the Y case), although it is still evident in the fact that films in O_2 decompose earlier than powders because in the latter there is gas (i.e. O_2) depletion in the inter-particles voids of the bulk [44]. This smooth behavior justifies TEA application as a solution stabilizer in thin film fabrication, upon the need to contrast the abrupt film shrinkage due to rapid decomposition.

Despite that, in the context of chemical solution deposition methods, where long-chain additives are used as stabilizers, the final decomposition temperatures and intermediate phases can play an important role in the final properties of the film, even when the final phases might not differ from the additive-free case.

5. Conclusions

In conclusion, we have shown that TA can be used to study complex solution behavior even in the form of films; in a FF-YBCO precursor solution with 5%TEA, TEA is expected to affect decomposition. Decomposition results in the formation of ethyl propionate in inert atmosphere, for both $YProp_3$ and $CuProp_2$. This reaction path prevents CuO reduction to Cu(0) in N_2. In humid atmosphere, the different behavior of the two metal carboxylates is reflected in the formation of the ester for $YProp_3$ and in the formation of the corresponding acid for $CuProp_2$, as a consequence of the preferred cleavage of the M—OC=O bond. Although TEA is responsible for smoother mass losses when its decomposition temperature and that of the metal carboxylate overlap, or when it is coordinated in a metalorganic complex, other effects need to be taken into account.

For example, the presence of TEA shifts the final decomposition temperature to higher values for the copper and yttrium case in O_2, but not for the barium case. Residual carbon at 500-600°C might be more important when compared to metal carboxylate solutions without TEA. Additionally, if less “carbon” is added to the solution in the form of long chain additives, less Cu(II) reduction (in the form of Cu and Cu_2O) will take place in humid O_2 during decomposition.

Clearly this study deals with relatively thick films (3-10 µm), but it can provide general trends for the study of YBCO obtained from CSD methods although based on thinner films (≤1µm).

Acknowledgments

This work was funded by Ministerio de Ciencia, Innovación y Universidades (grant numbers RTI2018-095853-B-C21 and RTI2018-095853-B-C22), by the Center of Excellence Severo Ochoa (SEV-2015-0496), the Generalitat of Catalunya (2017-SGR-1519). It was also supported by the European Union through the projects Eurotapes (EU-FP7 NMP-LA-2012-280432) and Ultrasupertape (ERC ADG-2014-669504). S.R. wishes to thank the University of Girona for the IF-UdG PhD grant.

Bibliography

[1] X. Obradors, T. Puig, S. Ricart, M. Coll, J. Gazquez, A. Palau, X. Granados, Growth , nanostructure and vortex pinning in superconducting YBa2Cu3O7 thin films based on trifluoroacetate solutions, Supercond. Sci. Technol. 25 (2012) 123001. doi:10.1088/0953-2048/25/12/123001.

[2] A. Rahman, Z. Rahaman, N. Samsuddoha, A Review on Cuprate Based Superconducting Materials Including Characteristics and Applications, Am. J. Phys. Appl. 3 (2015) 39–56. doi:10.11648/j.ajpa.20150302.15.

[3] T. Puig, J.C. Gonzáles, A. Pomar, N. Mestres, O. Castaño, M. Coll, J. Gásquez, F. Sandiumenge, S. Piñol, X. Obradors, The influence of growth conditions on the microstructure and critical currents of TFA-MOD YBa2Cu3O7 films, Supercond. Sci. Technol. 18 (2005) 1141–1150. doi:10.1088/0953-2048/18/8/020.

[4] A. Pomar, J. Gutiérrez, A. Palau, T. Puig, X. Obradors, Porosity induced magnetic granularity in epitaxial YBa2Cu3O7 thin films, Phys. Rev. B. 73 (2006). doi:10.1103/PhysRevB.73.214522.

[5] E. Bartolomé, F. Gömory, X. Granados, T. Puig, X. Obradors, Universal correlation between critical current density and normal-state resistivity in porous YBa2Cu3O7−x thin films, Supercond. Sci. Technol. 20 (2007) 895–899. doi:10.1088/0953-2048/20/10/001.

[6] W. Wu, F. Feng, K. Shi, W. Zhai, T. Qu, R. Huang, X. Tang, X. Wang, J.-C. Grivel, Z. Han, A Rapid Process of YBa2Cu3O7−δ Thin Film Fabrication Using Trifluoroacetate Metal Organic Deposition with Polyethylene Glycol Additive, Supercond. Sci. Technol. 26 (2013) 055013. doi:10.1088/0953-2048/26/5/055013.

[7] C. Ecjhao, K. Majid, R. Mushtaq, Synthesis , Characterization and Coordinating Behaviour of Aminoalcohol Complexes with Transition Metals, E-Journal Chem. 5 (2008) S969–S979. doi:10.1155/2008/680324.

[8] A.A. Naiini, V. Young, J.G. Verkade, G. Hall, New Complexes of Triethanolamine (TEA): Novel Structural Features of [Y(TEA)2](ClO4)3•3C5H5N AND [Cd(TEA)2](NO3)2, Polyhedron. 14 (1995) 393–400. doi:10.1016/0277-5387(95)93020-2.

[9] K.H. Whitmire, J.C. Hutchison, A. Gardberg, C. Edwards, Triethanolamine complexes of copper, Inorganica Chim. Acta. 294 (1999) 153–162. doi:10.1016/s0020-1693(99)00274-1.

[10] B. Kozlevčar, P. Šegedin, Structural Analysis of a Series of Copper (II) Coordination Compounds and Correlation with their Magnetic Properties, in: Croat. Chem. Acta, 2008: pp. 369–379.

[11] R.M. Escovar, J.H. Thurston, T. Ould-ely, A. Kumar, K.H. Whitmire, Synthesis and Characterization of New Mono-, Di-, and Trinuclear Copper(II) Triethanolamine-Carboxylate Complexes, Z. Anorg. Allg. Chem. 631 (2005) 2867–2876. doi:10.1002/zaac.200500204.

[12] K.D.B.Æ.P. Lommens, Æ.J.F.Æ.D. Vandeput, I. Van Driessche, Sol-gel chemistry of an aqueous precursor solution for YBCO thin films, J. Sol-Gel Sci. Technol. 52 (2009) 124–133. doi:10.1007/s10971-009-1987-1.

[13] B. Schoofs, D. Van de Vyver, P. Vermeir, J. Schaubroeck, S. Hoste, G. Herman, I. Van Driessche, Characterisation of the sol-gel process in the superconducting NdBa2Cu3O7-y system, J. Mater. Chem. 17 (2007) 1714–1724. doi:10.1039/b614149h.

[14] S.G. De de Ávila, M.A. Logli, J.R. Matos, Kinetic study of the thermal decomposition of monoethanolamine (MEA), diethanolamine (DEA), triethanolamine (TEA) and methyldiethanolamine (MDEA), Int. J. Greenh. Gas Control. 42 (2015) 666–671. doi:10.1016/j.ijggc.2015.10.001.

[15] S.B. Fredriksen, K. Jens, Oxidative degradation of aqueous amine solutions of MEA , AMP , MDEA , Pz : A review, Energy Procedia. 37 (2013) 1770–1777. doi:10.1016/j.egypro.2013.06.053.
[16] I. Zghal, J. Farjas, J. Camps, M. Dammak, P. Roura, Thermogravimetric measurement of the equilibrium vapour pressure : Application to water and triethanolamine, Thermochim. Acta. 665 (2018) 92–101. doi:10.1016/j.tca.2018.05.007.
[17] V.T. Yilmaz, Y. Topcu, A. Karadag, Thermal decomposition of triethanolamine and monoethanolethylenediamine complexes of some transition metal saccharinates, Thermochim. Acta. 383 (2002) 129–135. doi:10.1016/s0040-6031(01)00685-2.
[18] R.B. Mos, M. Nasui, T. Petrisor Jr, M.S. Gabor, R. Varga, L. Ciontea, T. Petrisor, Synthesis, crystal structure and thermal decomposition study of a new barium acetato-propionate complex, J. Anal. Appl. Pyrolysis. 92 (2011) 445–449. doi:10.1016/j.jaap.2011.08.007.
[19] Z. Lin, D. Han, S. Li, Study on thermal decomposition of copper(II) acetate monohydrate in air, J. Therm. Anal. Calorim. 107 (2012) 471–475. doi:10.1007/s10973-011-1454-4.
[20] M. Nasui, R.B. Mos, T. Petrisor Jr, M.S. Gabor, R.A. Varga, L. Ciontea, T. Petrisor, Synthesis, crystal structure and thermal decomposition of a new copper propionate [Cu(CH3CH2COO)2]·2H2O, J. Anal. Appl. Pyrolysis. 92 (2011) 439–444. doi:10.1016/j.jaap.2011.08.005.
[21] J. Grivel, Thermal decomposition of yttrium(III) propionate and butyrate, J. Anal. Appl. Pyrolysis. 101 (2013) 185–192. doi:10.1016/j.jaap.2013.01.011.
[22] J. Grivel, Thermal decomposition of lutetium propionate, J. Anal. Appl. Pyrolysis. 89 (2010) 250–254. doi:10.1016/j.jaap.2010.08.011.
[23] J. Grivel, Thermal decomposition of Ln(C2H5CO2)3•H2O (Ln=Ho,Er,Tm and Yb), J. Therm. Anal. Calorim. 109 (2012) 81–88. doi:10.1007/s10973-011-1745-9.
[24] S. Rasi, S. Ricart, X. Obradors, T. Puig, P. Roura, J. Farjas, Thermal decomposition of yttrium propionate: film and powder, J. Anal. Appl. Pyrolysis. 133 (2018) 225–233. doi:10.1016/j.jaap.2018.03.021.
[25] S. Rasi, F. Silveri, S. Ricart, X. Obradors, T. Puig, P. Roura-Grabulosa, J. Farjas, Thermal decomposition of CuProp2: In-situ analysis of film and powder pyrolysis, J. Anal. Appl. Pyrolysis. 140 (2019) 312–320. doi:10.1016/j.jaap.2019.04.008.
[26] S. Rasi, S. Ricart, X. Obradors, T. Puig, P. Roura-Grabulosa, J. Farjas, Radical and oxydative pathways in the pyrolysis of a barium propionate-acetate salt, J. Anal. Appl. Pyrolysis. 141 (2019) 104640. doi:10.1016/j.jaap.2019.104640.
[27] D.M. de Leeuw, C.A.H.A. Mutsaers, R.A. Steeman, E. Frikkee, H.W. Zandbergen, Crystal Structure and Electrical Conductivity of YBa4Cu3O8.5+∂, Phys. C. 158 (1989) 391–396.
[28] P. Vermeir, I. Cardinael, J. Schaubroeck, K. Verbeken, B. Michael, P. Lommens, W. Knaepen, D. Jan, K. De Buysser, I. Van Driessche, Elucidation of the Mechanism in Fluorine-Free Prepared YBa2Cu3O7-δ Coatings, Inorg. Chem. 49 (2010) 4471–4477. doi:10.1021/ic9021799.
[29] L. Soler, et al., Ultrafast transient liquid assisted growth of high current density superconducting films, Nat. Mater. (n.d.) submitted.
[30] H. Maeda, Y. Yanagisawa, Recent Developments in High-Temperature Superconducting Magnet Technology (Review), IEEE Trans. Appl. Supercond. 24 (2014) 1–12. doi:10.1109/TASC.2013.2287707.
[31] X. Obradors, T. Puig, Coated conductors for power applications: materials challenges, Supercond. Sci. Technol. 27 (2014) 44003–44019. doi:10.1088/0953-2048/27/4/044003.
[32] M. Nasui, T. Petrisor Jr, R.B. Mos, A. Mesaros, R.A. Varga, B.S. Vasile, T. Ristoiu, L. Ciontea, T. Petrisor, Synthesis , crystal structure and thermal decomposition kinetics of yttrium propionate, J. Anal. Appl. Pyrolysis. 106 (2014) 92–98. doi:10.1016/j.jaap.2014.01.004.
[33] M. Nasui, C. Bogatan (Pop), L. Ciontea, T. Petrisor, Synthesis, crystal structure modeling and thermal decomposition of yttrium propionate [Y2(CH3CH2COO)6·H2O]·3.5H2O, J. Anal. Appl. Pyrolysis. 97 (2012) 88–93. doi:10.1016/j.jaap.2012.05.003.
[34] M.S. Akanni, O.B. Ajayi, J.N. Lambi, Pyrolytic Decomposition of Some Even Chain Length Copper(II) Carboxylates, J. Therm. Anal. 31 (1986) 131–143. doi:10.1007/bf01913894.
[35] M.D. Judd, B.A. Plunkett, M.I. Pope, The thermal decomposition of calcium, sodium, silver and copper(II) acetates, J. Therm. Anal. 6 (1974) 555–563. doi:10.1007/BF01911560.
[36] W. Yaoyu, S. Qianl, S. Qizhenl, G. Yici, Z. Zhongyuan, Synthesis , thermal decomposition and crystal structure of Copper (II) α, β-unsaturated carboxylate with urea, Chinese Sci. Bull. 44 (1999) 602–605. doi:10.1007/bf03182717.
[37] X. Palmer, C. Pop, H. Eloussi, B. Villarejo, P. Roura, J. Farjas, A. Calleja, A. Palau, T. Puig, S. Ricart, Solution design for low-fluorine trifluoroacetate route to YBa2Cu3O7 films, Supercond. Sci. Technol. 29 (2016) 24002. doi:10.1088/0953-2048/29/2/024002.
[38] J.A.R. Cheda, M. V García, M.I. Redondo, S. Gargani, P. Ferloni, Short chain copper(II) n-alkanoate liquid

crystals, Liq. Cryst. 31 (2004) 1–14. doi:10.1080/02678290310001628500.
[39] Y.H. Chung, H.H. Wei, Y.H. Liu, G.H. Lee, Y. Wang, Reinvestigation of the crystal structure and cryomagnetic behaviour of copper(II) propionates, Polyhedron. 17 (1998) 449–455. doi:10.1016/s0277-5387(97)00367-7.
[40] H.Ö. H. Içbudak, V.T. Yilmaz, Thermal decompositions of some divalent transition metal complexes of triethanolamine, J. Therm. Anal. 44 (1995) 605–615. doi:10.1007/BF02636280.
[41] A. Karadag, V.T. Yilmaz, C. Thoene, Di- and triethanolamine complexes of Co(II), Ni(II) and Zn(II) with thiocyanate: synthesis, spectral and thermal studies. Crystal structure of dimeric Cu(II) complex with deprotonated diethanolamine, [Cu2(μ-dea)2(NCS)2], Polyhedron. 20 (2001) 635–641. doi:10.1016/S0277-5387(01)00720-3.
[42] J.-C.C. Grivel, Thermal decomposition of yttrium(III) propionate and butyrate, J. Anal. Appl. Pyrolysis. 101 (2013) 185–192. doi:10.1016/j.jaap.2013.01.011.
[43] P. Torres, P. Norby, J. Grivel, Thermal decomposition of barium valerate in argon, J. Anal. Appl. Pyrolysis 116. 116 (2015) 120–128. doi:10.1016/j.jaap.2015.09.018.
[44] P. Roura, J. Farjas, H. Eloussi, L. Carreras, S. Ricart, T. Puig, X. Obradors, Thermal analysis of metal organic precursors for functional oxide preparation: Thin films versus powders, Thermochim. Acta. 601 (2015) 1–8. doi:10.1016/j.tca.2014.12.016.
[45] W.E. Wallace, Infrared Spectra, in: P.J. Linstrom, W.G. Mallard (Eds.), NIST Chem. WebBook, NIST Stand. Ref. Database Number 69, Institute of Standards and Technology, Gaithersburg MD, 20899, n.d. doi:https://doi.org/10.18434/T4D303.
[46] W.E. Wallace, Mass spectra, in: P.J. Linstrom, W.G. Mallard (Eds.), NIST Chem. WebBook, NIST Stand. Ref. Database Number 69, National Institute of Standards and Technology, Gaithersburg MD, 20899, n.d. doi:https://doi.org/10.18434/T4D303.

Figure captions

Fig. 1: (a) FTIR analysis and (b) XRD pattern of some quenched films during decomposition of sol. **B** (Ba/TEA) in humid O_2 at 5°C/min.

Fig. 2: TG-DSC analysis of $BaProp_2$/TEA film (~5 µm from sol. **B**) decomposition in humid O_2 at 5°C/min. Inset: Infrared spectra of gas species detected from TG-FTIR analysis. Horizontal dashed lines: theoretical final mass for the formation of the indicated products.

Fig. 3: Chemical characterization of quenched samples during the thermal decomposition of $CuProp_2$/TEA (sol. **C**) at 5°C/min in humid O_2. (a) FTIR analysis and (b) XRD patterns.

Fig. 4: TG-DSC-FTIR analysis of $CuProp_2$/TEA film (~1 µm, sol. **C**) decomposition in humid O_2 at 5°C/min. Dotted line: TG curve relative to sol. **C'**. The absorbance peaks are plotted choosing the evolution in temperature of a characteristic wavenumber for each volatile. Horizontal dashed lines: theoretical final mass for the formation of the indicated products.

Fig. 5: TG-FTIR analysis (top graph) of powders from sol. **C** decomposed in atmospheric pressure of N_2 (details in Supp. Info, Fig. S6); EGA-MS analysis (bottom graph) showing the main fragments coming from decomposition in vacuum of $CuProp_2$/TEA at 5°C/min. FTIR and MS reference spectra are based on [45,46].

Fig. 6: TG-DSC analysis of $YProp_3$/TEA film from sol. **A** (solid lines) during decomposition in humid O_2 at 5°C/min, with the relative time-evolution of the main volatiles detected by TG-FTIR analysis from sol. **A'** (dotted line; the relative FTIR spectra at selected temperatures are reported in Fig. S5). Horizontal dashed lines: theoretical final mass for the formation of the indicated products.

Fig. 7: (a) FTIR analysis and (b) XRD patterns of quenched samples during the thermal decomposition at 5°C/min and in humid O_2 of $YProp_3$/TEA (sol. **A**) shown in Fig. 6.

Fig. 8: TG-FTIR (top graph, with FTIR spectra in inset) and EGA-MS results (bottom) relative to the thermal decomposition of $YProp_3$/TEA (sol. **A**) at 5°C/min in N_2 and vacuum, respectively. Detailed IR spectra and enlargement of inset can be found in Fig. S6. FTIR and MS assignments based on [45,46].

Tables

Compound	Found (expected), mass %	
	wt%C	wt%H
A (Y/TEA, 600°C)	1.3 (0)	- (0)
A (Y/TEA, 500°C)	2.6	0.4
B (Ba/TEA, 500°C)	6.7 (6.09)	- (0)
C (Cu/TEA, 500°C)	- (0)	- (0)

Table 1: Elemental analysis results for the decomposition products of metal carboxylate/TEA solutions in humid O_2. (-) values inferior to detection limits. Expected values correspond to yttria, barium carbonate and copper oxide.

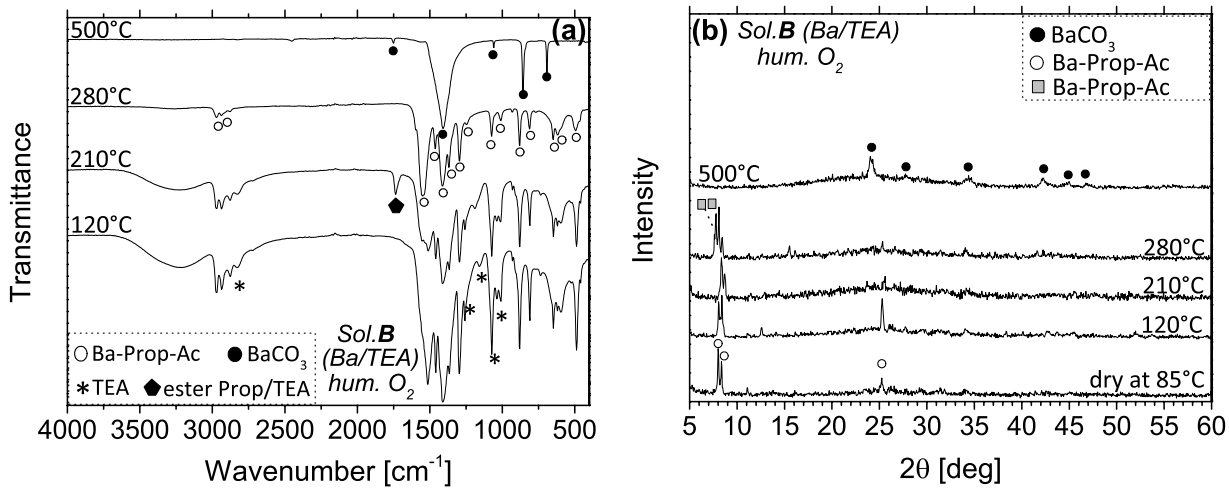
(a)
500°C
280°C
210°C
120°C
Transmittance
Ba-Prop-Ac
BaCO3
TEA
ester Prop/TEA
Sol.B (Ba/TEA) hum. O2
4000 3500 3000 2500 2000 1500 1000 500
Wavenumber [cm-1]
(b) Sol.B (Ba/TEA) hum. O2
BaCO3
Ba-Prop-Ac
Ba-Prop-Ac
500°C
280°C
210°C
120°C
dry at 85°C
Intensity
5 10 15 20 25 30 35 40 45 50 55 60
2θ [deg]

Fig1

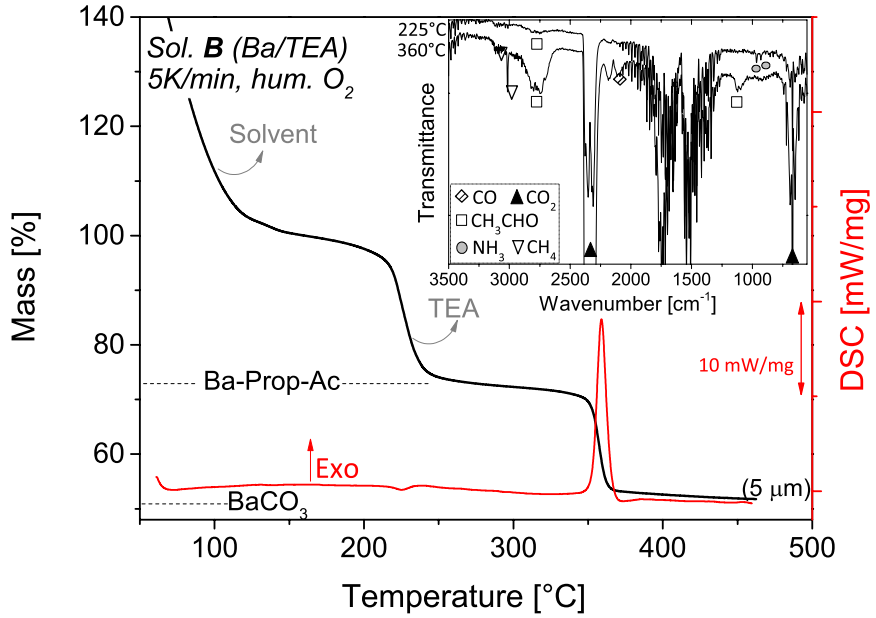
Sol. B (Ba/TEA)
5K/min, hum. O2
Solvent
TEA
Ba-Prop-Ac
Exo
BaCO3
225°C
360°C
Transmittance
CO CO2
CH3CHO
NH3 CH4
3500 3000 2500 2000 1500 1000
Wavenumber [cm-1]
10 mW/mg
(5 μm)
Mass [%]
DSC [mW/mg]
140 120 100 80 60
100 200 300 400 500
Temperature [°C]

Fig2

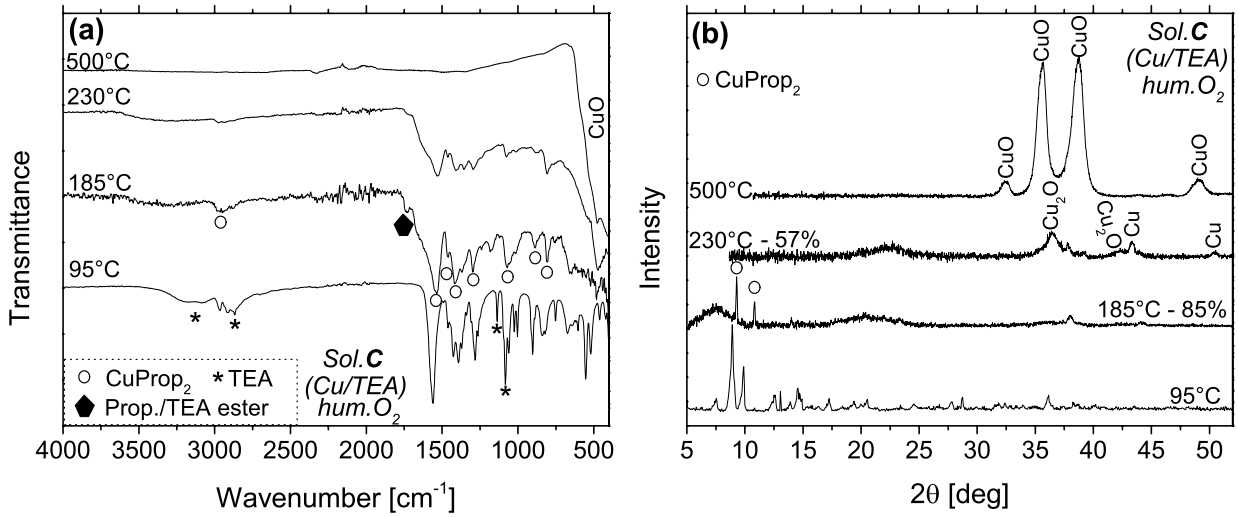

Fig3

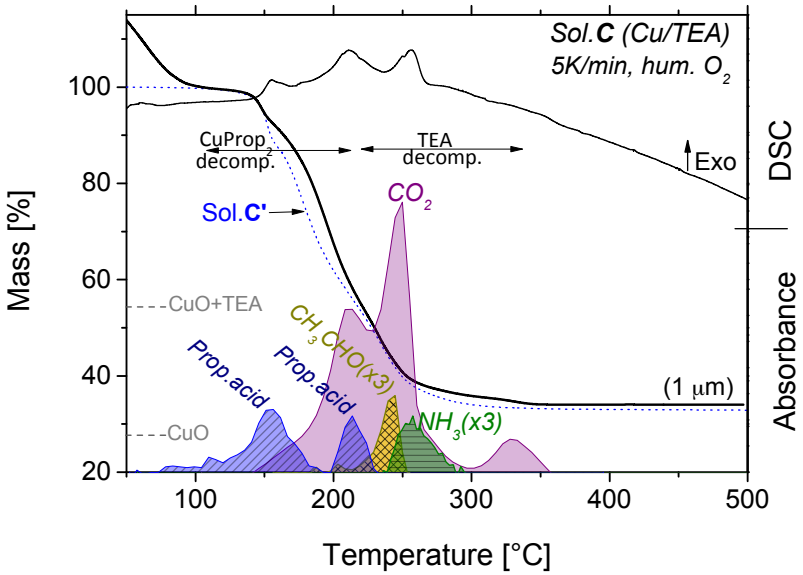

Fig4

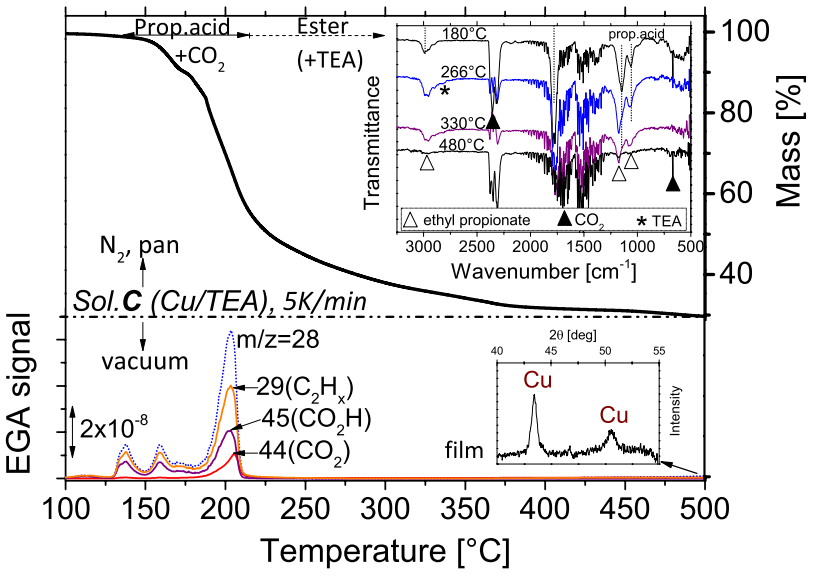

Fig5

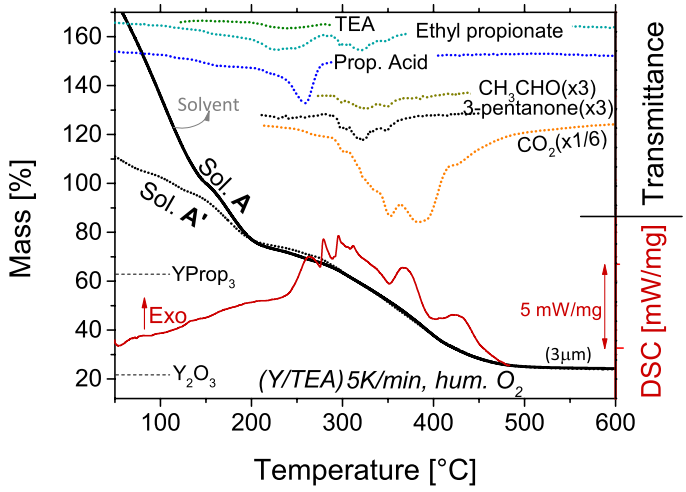

Fig6

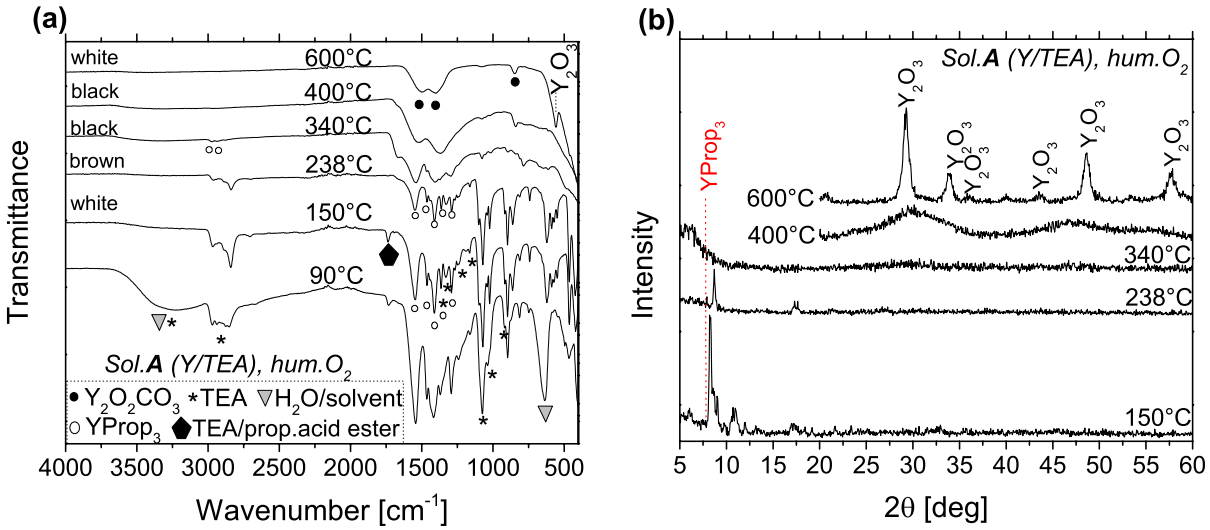

Fig7

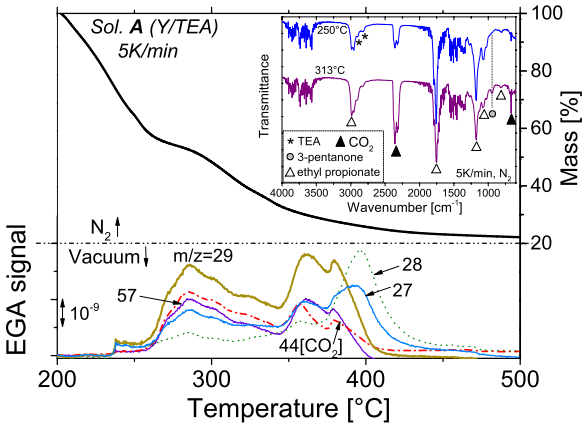

Fig8

SUPPORTING INFORMATION

Triethanolamine (TEA) effect on the pyrolysis of metal propionate-based solutions shown by thermal analysis

Silvia Rasi[1,2], Susagna Ricart[2], Xavier Obradors[2], Teresa Puig[2], Pere Roura-Grabulosa[1] and Jordi Farjas[1]

[1] University of Girona, Campus Montilivi, Edif. PII, E17003 Girona, Catalonia, Spain
[2] Institut de Ciència de Materials de Barcelona, ICMAB – CSIC, Campus UA Barcelona, E-08193 Bellaterra, Catalonia, Spain

ADDITIONAL FTIR and XRD SPECTRA

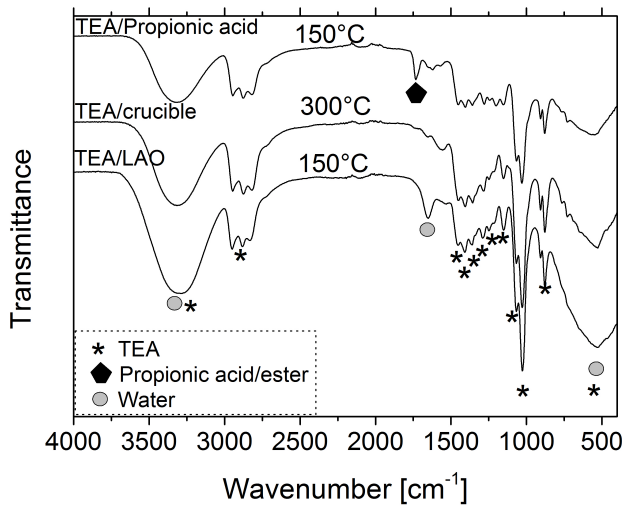

***Fig. S1**: FTIR analysis of (bottom spectrum) TEA decomposed to 150 °C and (center spectrum) to 300°C, and FTIR analysis of (top spectrum) a solution of TEA in propionic acid decomposed to 150°C. The probable esterification reaction between the -OH terminal groups of TEA and the carboxylic bond of the propionic acid results in the peak at ~1736 cm^{-1}, identified with the symbol: ⬟ .*

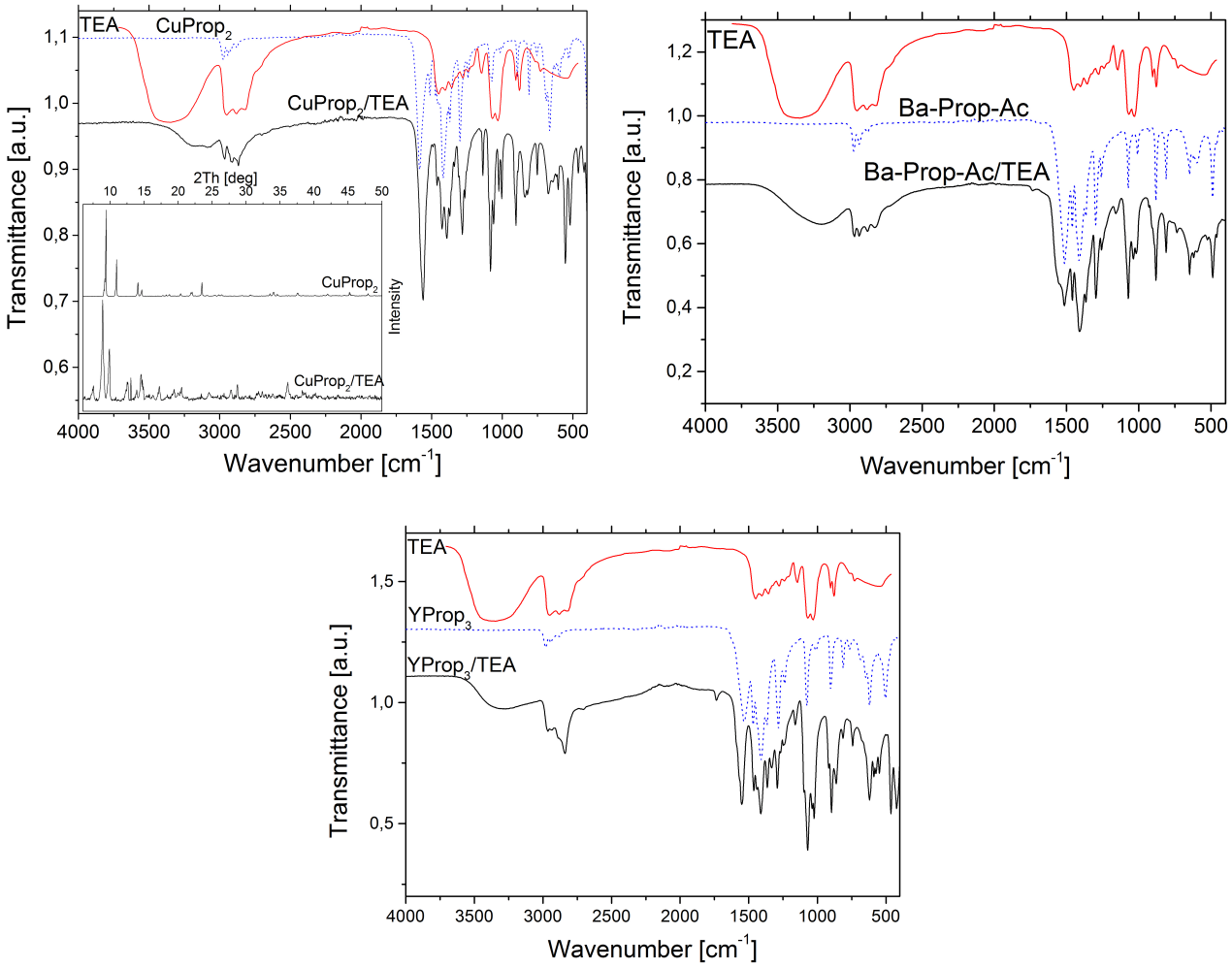

***Fig. S2**: Comparison between the FTIR spectrum of the metal carboxylate salt, the FTIR spectrum of TEA and that of $MProp_x$/TEA, for all three cases under study (Cu, Y, Ba).*

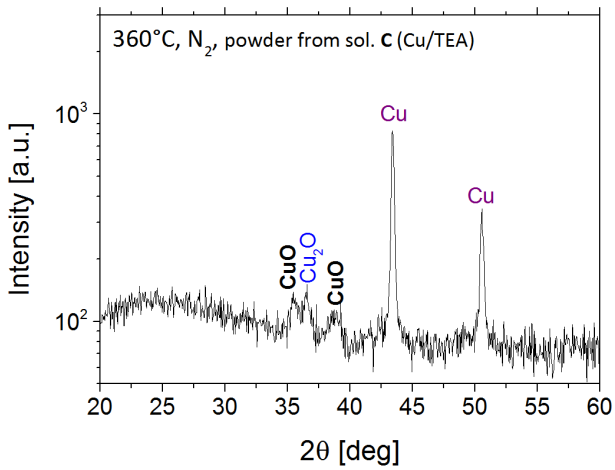

***Fig. S3**: XRD analysis of the powder obtained from sol. **C** ($CuProp_2$/TEA) decomposed in N_2. The sample was heated at 5°C/min in a pan and quenched at 360°C prior to the XRD analysis.*

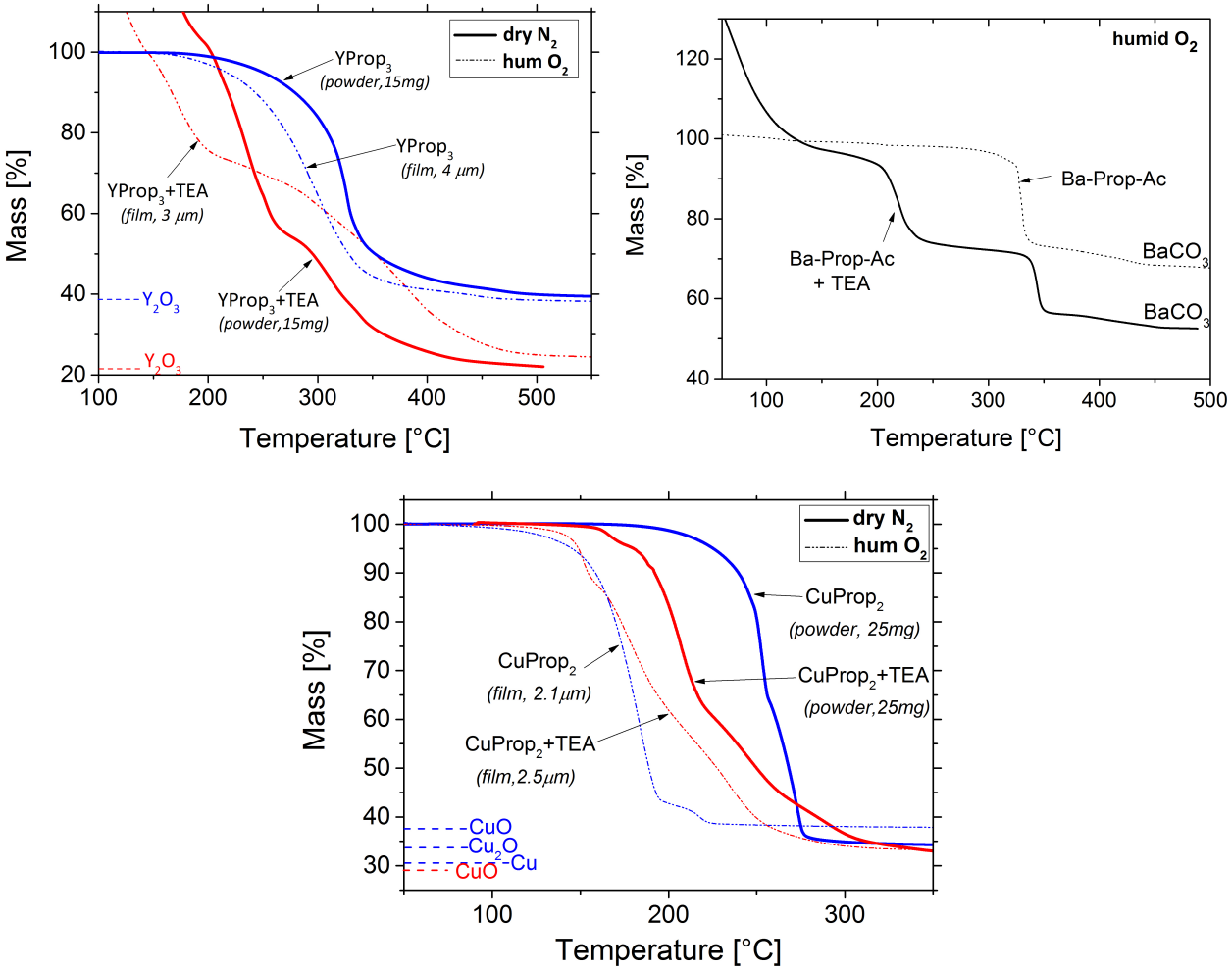

***Fig. S4**: Each figure compares the thermogravimetric curve of $MProp_x$ with that of $MProp_x$/TEA in a specific furnace atmosphere (dry N_2 and humid O_2). Decomposition ends at higher temperature for yttrium and copper with TEA decomposed in humid O_2, but it does not show substantial differences for the barium case. The shift of the decomposition temperature upon a change of atmosphere is less significant for the $MProp_x$/TEA case with respect to the isolated $MProp_x$.*

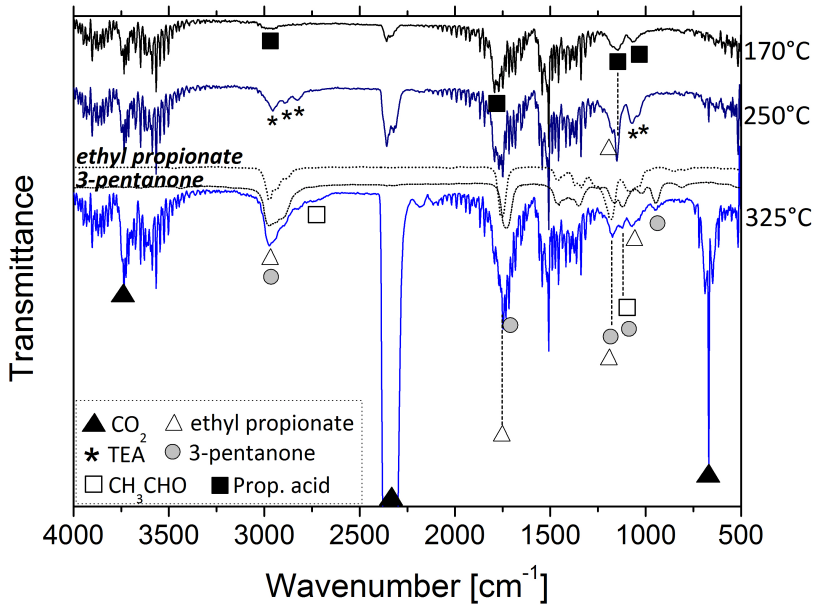

***Fig. S5**: Infrared gas spectra recorded at different temperatures during the TG-FTIR experiment relative to sol. **A'** (Y/TEA case) in humid O_2. The first step involves release of propionic acid with a maximum at ~250°C; at the same temperature, TEA and ethyl propionate are detected; this is followed at higher temperatures (>300°C) by acetaldehyde, ethyl propionate, 3-pentanone and CO_2. Dotted IR curve: reference spectra for the volatiles indicated.*

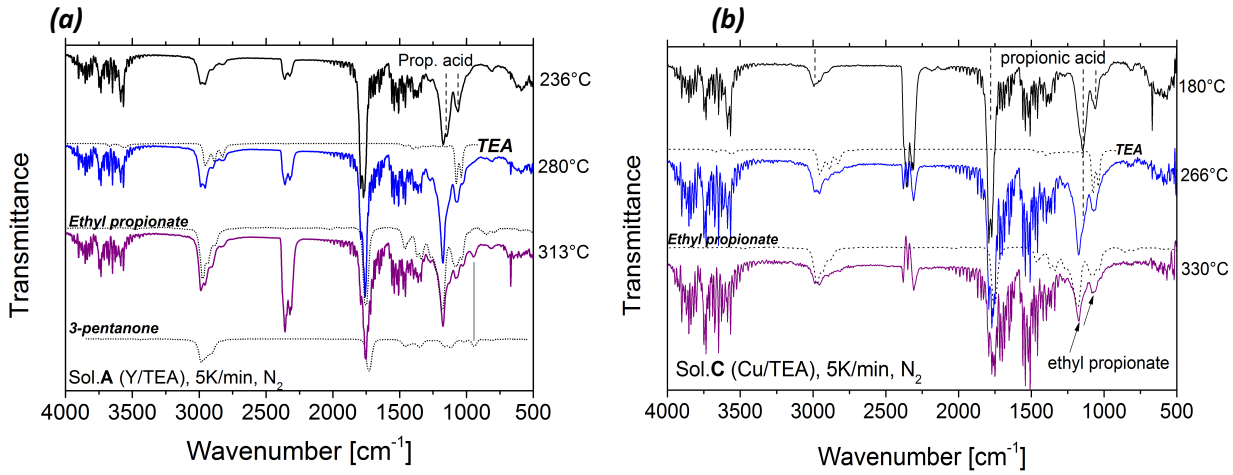

***Fig. S6**: EGA-IR spectra of the gaseous species detected at given temperatures during the TG-FTIR experiment relative to **(a)** sol. **A** and **(b)** sol. **C** (performed in N_2 and 70-µl-Al_2O_3 pan). Dotted IR curves: reference spectra of some volatiles. The TG-FTIR analysis shows that the main volatiles consist of TEA and ethyl propionate, while 3-pentanone contribution is residual in sol. **A**.*

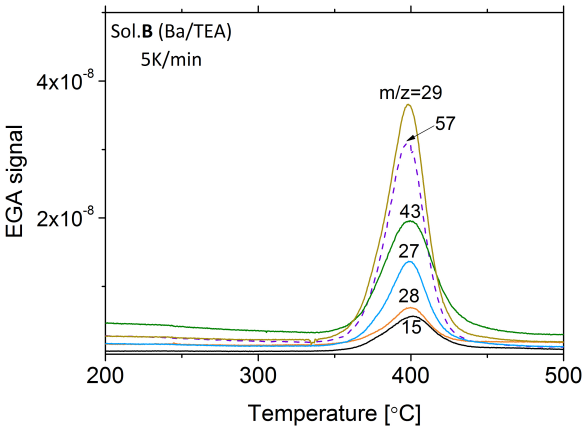

***Fig. S7**: EGA-MS of solution **B** (Ba/TEA) decomposed at low total pressures (P_{TOT} ~10^{-7} bar), showing the same decomposition volatiles as for the $BaProp_2$ case without TEA. This is in agreement with the fact that there is no complexation Ba^{2+}-TEA that may help reduce TEA volatilization; thus, TEA evaporates and condensates along the path before decomposition of $BaProp_2$ can start, explaining why TEA is not detected by EGA-MS. The final product is black. Conversely, solutions **A** and **C** show different behavior than their corresponding metal propionates without TEA decomposed in vacuum.*

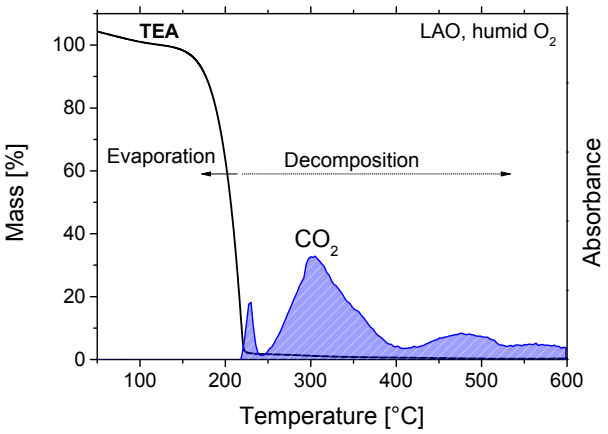

***Fig. S8**: TG-FTIR analysis of TEA deposited on a substrate and decomposed in humid O_2 at 5°C/min. Before ~250°C, the main contribution to the mass loss comes from the evaporation process. At higher temperatures (>230°C), the remaining TEA decomposes, and CO_2 is detected by gas infrared.*